Proceedings of the Korean Nuclear Society Spring Meeting
Kwangju, Korea, May 2002

Comparison of Eddy Viscosity Models and Reynolds Stress Model for the Prediction of Flow in a Rod Bundle with the Flow Deflector

Wang Kee In, Dong Seok Oh, Tae Hyun Chun
Korea Atomic Energy Research Institute
P.O. Box 105, Yusong, Daejeon, Korea, 305-600

Abstract

A computational fluid dynamics analysis is conducted to evaluate the prediction performance of the standard and RNG $k-e$ eddy viscosity models, and differential stress model (DSM). A 5x5 rod array with the split vane is simulated and the numerical predictions are compared with the experimental results where applicable. The curvature-compensated convective transport (CCCT) scheme is used to discretise the convection term. There is a negligible difference in the prediction performance between the standard and RNG $k-e$ models. DSM was found to more accurately predict characteristics of turbulent flow in the fuel bundle with the flow-deflecting vane.

1. Introduction

The fuel bundle used in a pressurized water reactor (PWR) is a rod bundle whose rod-rod clearance is maintained by the grid spacer. The coolant moves axially through the subchannels formed between neighboring fuel rods and between the peripheral fuel rods and the flow tube. Attempts have been made to increase the departure from nucleate boiling (DNB) performance by providing the fuel bundle with integral flow-deflecting vanes. The onset of film boiling on the surfaces of the fuel rods is one of the operating limitations on a PWR to avoid failure of the fuel rod. These vanes can improve the DNB performance by increasing coolant mixing and the rod heat transfer ability downstream of the vanes. Figure 1 illustrates the typical nuclear fuel bundle of a pressurized water reactor and the grid spacer with rod support features (spring and dimple) and mixing vane. The size, shape, bend angle, and location of the vanes should be optimized to maximize the benefit of the vanes. It is essential to accurately predict the turbulent flow in the fuel bundle for the optimal design of flow-mixing promoters.

There are few experimental and numerical studies on the turbulent flow in the nuclear fuel bundle with the mixing vane since it is complex flow. The experimental studies (Shen et al. 1991, Karoutas et al. 1995, and Yang and Chung 1996) measured turbulent flow characteristics in the rod bundle with a split-vane flow deflector. They found a swirling flow in the subchannel and a cross flow between the subchannels caused by the split vane. Recently, the numerical analyses (Imaizumi et al. 1995, Karoutas et al. 1995, Ikeda and Hoshi 2001, and In 2001) were reported to investigate the characteristics of turbulent flow in the rod bundle with the mixing devices. Using the computational fluid dynamics (CFD) method, they performed a three-dimensional flow analysis for the optimal design of the mixing devices on the grid spacer of the PWR fuel bundle. The turbulence model used in these CFD analyses is the standard $k-e$ turbulence model of Launder and Spalding (1974) since it converges well for the complex turbulent flow in a nuclear fuel bundle. The numerical studies confirmed that swirl and cross flow caused by the mixing vane are important mechanisms of coolant mixing.

The objective of this study is to evaluate the effect of turbulence models in the prediction of flow in a rod bundle with the split vane. The turbulence models examined are the standard and RNG $k-e$ eddy viscosity

models, and differential Reynolds stress model.

2. Turbulence Models

The equations of motion are averaged over a time period producing what are known as Reynolds equations. The Reynolds averaged Navier-Stokes (RANS) equations include an additional set of terms, the Reynolds stresses, that have to be accurately represented in terms of known quantities. Turbulence modeling is required to achieve closure of the Reynolds equations by supplementary transport equations. The closure models range from the eddy viscosity model (EVM) to full second moment closure models which represent each component of the Reynolds stress tensor on the mean flow.

The standard $k-e$ model of Launder and Spalding (1974) uses an eddy viscosity hypothesis for the turbulence. The transport equations for the turbulent kinetic energy k and the dissipation rate of k, e are

$$r\frac{\partial k}{\partial t}+rU_j\frac{\partial k}{\partial x_j}=t_{ij}\frac{\partial U_i}{\partial x_j}-re+\frac{\partial}{\partial x_i}\left[\left(m+m_t/s_k\right)\frac{\partial k}{\partial x_j}\right], \tag{1}$$

and

$$r\frac{\partial e}{\partial t}+rU_j\frac{\partial e}{\partial x_j}=C_{e1}\frac{e}{k}t_{ij}\frac{\partial U_i}{\partial x_j}-C_{e2}r\frac{e^2}{k}+\frac{\partial}{\partial x_i}\left[\left(m+m_t/s_e\right)\frac{\partial e}{\partial x_j}\right], \tag{2}$$

where

$$t_{ij}=-r\overline{u_i'u_j'}=m_t\left(\frac{\partial U_i}{\partial x_j}+\frac{\partial U_j}{\partial x_i}\right)-\frac{2}{3}rkd_{ij} \tag{3}$$

$$m_t=rC_m\frac{k^2}{e}. \tag{4}$$

The closure coefficients for the standard $k-e$ model are as follows.

$$C_m=0.09,\ C_{e1}=1.44,\ C_{e2}=1.92,\ s_k=1.0,\ s_e=1.3 \tag{5}$$

The Renormalization Group (RNG) model is an alternative to the standard $k-e$ model proposed by Yakhot and Orzag (1986). They applied Renormalization Group theory to the Navier-Stokes equations and derived a two equation $k-e$ model only through a modification to the equation for e. The only revision to the standard equation for the RNG model is the inclusion of the extra term C_{1RNG} and the inclusion of revised model constants:

$$r\frac{\partial e}{\partial t}+rU_j\frac{\partial e}{\partial x_j}=\left(C_{e1}-C_{1RNG}\right)\frac{e}{k}t_{ij}\frac{\partial U_i}{\partial x_j}-C_{e2}r\frac{e^2}{k}+\frac{\partial}{\partial x_i}\left\{\left(m+m_t/s_e\right)\frac{\partial e}{\partial x_j}\right\} \tag{6}$$

where

$$C_{1RNG}=\frac{h\left(1-\frac{h}{h_o}\right)}{1+bh^3} \tag{7}$$

and

$$h=\left(\frac{P}{m_t}\right)^{1/2}\frac{k}{e}. \tag{8}$$

h_o and b are additional model constants and P is the shear part of the turbulence production, that is the first term in the right hand side of eq. (1). The model constants are given below.

$$h_o = 4.38,\ b = 0.012\ . \tag{9}$$

A more complex version of the RANS equations is the differential stress model (DSM) of Launder et al. (1975). It is based on exact transport equations for the individual Reynolds stresses derived from the Navier-Stokes equations. The exact differential equations describing the behavior of the Reynolds-stress tensor t_{ij} and dissipation rate e for an incompressible fluid are

$$\begin{aligned}\frac{\partial t_{ij}}{\partial t} + U_k \frac{\partial t_{ij}}{\partial x_k} &= -t_{ik}\frac{\partial U_j}{\partial x_k} - t_{jk}\frac{\partial U_i}{\partial x_k} + \frac{2}{3} r e d_{ij} - \Pi_{ij} \\ &+ C_s \frac{\partial}{\partial x_k}\left(\frac{k}{e}\left(t_{im}\frac{\partial t_{jk}}{\partial x_m} + t_{jm}\frac{\partial t_{ik}}{\partial x_m} + t_{km}\frac{\partial t_{ij}}{\partial x_m}\right)\right)\end{aligned} \tag{10}$$

and

$$r\frac{\partial e}{\partial t} + r U_j \frac{\partial e}{\partial x_j} = C_{e1}\frac{e}{k}t_{ij}\frac{\partial U_i}{\partial x_j} - C_{e2}\, r\frac{e^2}{k} - C_e\frac{\partial}{\partial x_k}\left(\frac{k}{e}t_{km}\frac{\partial e}{\partial x_m}\right) \tag{11}$$

where Π_{ij} is the pressure-strain correlation using the closure coefficients, C_1 and C_2. The values of the closure coefficients for the Launder, Reece and Rodi model (1975) are

$$C_1 = 1.8,\ C_2 = 0.60,\ C_s = 0.11,\ C_e = 0.18\ . \tag{12}$$

3. Numerical Method

3.1 CFD modeling

A CFD code, CFX-4.4, developed by AEA Technology is used to model the 5x5 rod array with the split vane on the grid spacer which was used in the experiments (Karoutas et al. 1995 and Yang and Chung 1996). The CFD model simulates one grid span of the test rod array. The rod diameter and pitch are 9.53 mm and 12.7 mm, respectively. Body-fitted and non-staggered grid systems were used to deal with complex geometries. A multi-block method is used to construct the three-dimensional CFD model consisting of 3600 structured blocks. The spacer and mixing vanes are treated as infinite thin surfaces. The other fuel spacer elements such as the spring and dimples are neglected for simplicity because their effect on the flow mixing is judged to be minimal only inside and near the grid spacer. Figure 2 shows the CFD models of the 5x5 rod array and the split-vane grid.

Figure 3 shows the computational grid which is optimized through the grid convergence test. It was generated with 122 nodes along the side boundaries of the 5x5 rod array, 18 nodes in a rod-to-rod gap and 60 nodes in the axial direction. Total number of grids is 989,040 hexahedral cells for the entire CFD domain. A fine grid is used near the grid spacer and the rod surfaces. The grid size in non-dimensional wall unit (y^+) was calculated to be 20-35, which is the closest distance from the rod surface. A non-uniform grid was also used in the axial (main flow) direction with the fine grid near the inlet boundary and the mixing vane, and the coarse grid near the outlet boundary.

3.2 Boundary conditions

The grid span of a PWR fuel bundle is approximately 40 times the hydraulic diameter (~12 mm) of the rod bundle. Since one grid span is modeled in this analysis, the numerical simulation starts at 80 mm upstream and 500 mm downstream of the top of the grid spacer. Preliminary calculations were conducted with fully developed and uniform inlet boundary conditions. The fully developed inlet boundary conditions were taken from a model without a grid spacer. Velocities, turbulent kinetic energy and turbulent dissipation rate were transferred from the outlet in the no spacer case to the inlet in the simulations with the spacer. The inlet boundary conditions showed a negligible difference in the flow characteristics downstream of the spacer which may depend largely on the flow deflecting vanes on the grid spacer. Therefore, the uniform inlet boundary conditions were used in these CFD simulations. The turbulent parameters at the inlet boundary were estimated using bulk velocity and hydraulic diameter of the rod bundle.

A constant pressure and zero normal gradients of velocity and turbulent parameters were applied at the outlet boundary since it is far downstream of the spacer. The side boundary of the 5x5 rod array model is set to a non-slip condition since it is bounded by the housing wall. A no-slip condition was also used at the rod surface and the grid spacer.

3.3 Calculation procedure

The CFD code CFX-4.4 is used to solve the turbulent flow in a rod bundle with the split vane. The SIMPLEC algorithm is used to solve the velocity-pressure coupling. SIMPLEC is a modification of SIMPLE which differs in its derivation of a simplified momentum equation. The linearised difference equation for the pressure-correction is solved by the algebraic multi-grid method. The curvature-compensated convective transport (CCCT) differencing schemes was used to discretise the convection term. CCCT (Gaskell and Lau 1988) is a modification of the QUICK scheme which strictly preserves the boundedness of a convected scalar transport variable. CCCT is essentially third-order accurate.

The turbulence models used in this study are the standard and RNG $k-e$ models, and differential stress model. The standard wall functions using a universal law of the wall were applied to specify the turbulence in the near-wall region. The standard under-relaxation method was used to obtain a converged solution. The calculation was performed on HP9000 C180/C200 workstations (PA8000 CPU, 1 GB RAM) and terminated when the residual for the mass equation (sum of the absolute values of the net mass flux into or out of every cell in the flow field) is less than 0.05% of the total inlet mass flow rate. Meeting this criteria using CCCT differencing and the DSM was found to be very difficult. Hence, the convergence criteria increased to 0.5% for the calculations with CCCT differencing and the DSM. Approximately 1000 iterations were necessary to obtain a converged solution. The working fluid is water at room pressure and temperature, and the bulk inlet velocity (U_{bulk}) is 6.79 m/sec.

4. Results and Discussion

Figure 4 illustrates the velocity vectors in the 5x5 rod array with the split vane using the standard $k-e$ model and DSM. Both turbulence models predict a large cross flow between the subchannels and a skewed elliptic swirl in the internal subchannels near the spacer (z=25 mm downstream of the spacer) caused by the split vane. They predict negligibleswirl and cross flow in the wall and corner subchannels since the mixing vanes do not exist on the external side boundaries. DSM predicts slightly larger swirl than the standard $k-e$ model. Both the standard $k-e$ model and DSM predicted that the cross flow diminishes and the swirl inside the subchannel becomes dominant further downstream. Further downstream of the spacer, it is noted that DSM presents a remarkably larger swirl than the standard model. The velocity vectors by the RNG $k-e$ model are not presented because they are practically identical to those by the standard model.

The axial and lateral mean velocities were predicted along the horizontal centerline of the subchannels in the second row of the rod array and compared to the measurements. Figure 5 shows the comparison of axial velocity at two axial locations downstream of the spacer. The three turbulence models give almost identical velocity distributions which are different from the measured one near the spacer (13 mm downstream of the spacer). Far downstream of the spacer (464 mm downstream), DSM shows a more developed profile of the axial velocity, i.e., higher maximum velocities at the center of each subchannel than those of the standard and RNG $k-e$ models. There is no difference in the axial velocity prediction between the standard and RNG $k-e$ models.

Figure 6 shows the predicted and measured distributions of lateral mean velocity along the horizontal centerline of the subchannel at 13 mm and 464 mm downstream of the spacer. The three turbulence models resulted in mostly the same distributions near the spacer showing a good agreement with the measurement. However, a significant difference in the predictions between the turbulence models can be noted far downstream where the mixing-vane effect is disappears. The RNG $k-e$ model appears to predict slightly higher lateral velocity than the standard model. DSM resulted in remarkably higher predictions than the $k-e$ models. The CFD calculations show slightly higher value than the measured one.

Figure 7 shows the distribution of the cross-flow velocity in the gaps between the subchannels in the first row and the second row of the 5x5 rod array. It shows a significant amount of cross flow between the internal subchannels (-1.0 < x/Pitch < 3.0) but a small cross flow between the wall subchannels (x/Pitch < -1.0, 3.0 < x/Pitch). It can be noted that the standard and RNG $k-e$ models predict a slightly larger cross flow in the internal gaps than DSM.

Figure 8 compares the axial variations of axial turbulence intensity at the center and the gap of the central subchannel along with the experimental results by Yang and Chung (1996). The axial (main flow direction) turbulence intensity for the $k-e$ models was estimated from the computed turbulent kinetic energy by assuming that the axial turbulent fluctuations contribute about 60% of the turbulent kinetic energy. The standard and RNG $k-e$ models predicted a significant increase of the turbulence intensity at the center of the subchannel near the spacer due to the mixing vane and a rapid decrease further downstream of the spacer. The axial turbulence intensity at the center of the subchannel near the spacer (z < 200) is excessively over-predicted by the $k-e$ models and slightly under-predicted by DSM. Far downstream (z > 300), the predictions by the $k-e$ models and DSM show good agreement with the measured one. The turbulence intensity at the gap between the subchannels is under-predicted by all of the turbulence models close to the spacer (z < 50). DSM shows the prediction agreed well with the measured one while the $k-e$ models over-predict further downstream.

5. Conclusion

Computational fluid dynamics calculations were performed to evaluate the adequacy of turbulence models for turbulent flow in a nuclear fuel bundle with the mixing vane on the grid spacer. This CFD study used two eddy viscosity models (standard and RNG $k-e$ models) and Reynolds stress model. The CCCT scheme (third-order differencing) was used to discretise the convection term. The standard and RNG $k-e$ models show almost the same prediction performance in the rod-bundle flow. DSM was found to result in more accurate predictions of axial and lateral mean velocities, especially far downstream where the mixing-vane effect is negligible. DSM also shows a more reasonable prediction of the turbulence variation downstream of the mixing vane. For more complete evaluation of turbulence models, it is necessary to compare the CFD predictions with the experimental results, specifically on the turbulence parameters in a rod array in the future.

Acknowledgments

The authors express their appreciation to the Ministry of Science and Technology of Korea for financial support.

Nomenclature

k	Turbulent kinetic energy, $k = \frac{u_i' u_i'}{2}$
$\overline{u_i' u_j'}$	Reynolds stresses
U	The mean velocity
x_i	The coordinate direction
d_{ij}	Kronecker delta
e	Dissipation rate of k
r	Fluid density
m	Dynamic viscosity
s_k, s_e	*Turbulent Prandtl number for* k *and* e

References

AEA Technology, 2001. CFX-4.4: Solver, Oxfordshire, UK.

Gaskell P. H. and Lau A. K. C., 1988. Curvature-compensated transport: Smart, a new boundedness-preserving transport algorithm. Int. Journal for Numerical Methods in Fluids **8**, 617-641.

Ikeda K. and Hoshi M., 2001. Development of Mitsubishi high thermal performance grid 1 – CFD applicability for thermal hydraulic design. 9th Int. Conference on Nuclear Engineering, Nice, France, April 8-12.

Imaizumi M., Ichioka T., Hoshi M., Teshima H., Kobayashi H., and Yokoyama T., 1995. Development of CFD method to evaluate 3-D flow characteristics for PWR fuel assembly. Trans. of the 13th International Conference on SMiRT, Porto Alegre, Brazil, August 13-18.

In W. K., 2001. Numerical study of coolant mixing caused by the flow deflectors in a nuclear fuel bundle. Nuclear Technology **134**, 187-195.

Karoutas Z., Gu C.Y. and Scholin B., 1995. 3-D flow analyses for design of nuclear fuel spacer. Proc. of the 7th Int. Meeting on Nuclear Reactor Thermal-Hydraulics, New York, United Sates, September 10-15.

Launder B. E., Reece G. J. and Rodi W., 1975. Progress in the development of a Reynolds stress turbulence model. Journal of Fluid Mechanics **68**, 537-566.

Launder B. E. and Spalding D. B., 1974. The numerical computation of turbulent flows. Computational Methods in Applied Mechanics and Engineering **3**, 269-289.

Shen Y. F., Cao Z. D., and Lu Q. G., 1991. An investigation of crossflow mixing effect caused by grid spacer with mixing blades in a rod bundle. Nuclear Engineering and Design **125**, 111-119.

Yakhot V. and Orsag S. A, 1986. Renormalization Group analysis of turbulence: Basic theory. Journal of Science and Computing **1**, 3-51.

Yang S. K. and Chung M. K., 1996. Spacer grid effects on turbulent flow in rod bundles. Journal of the Korean Nuclear Society **28**(1), 56-71.

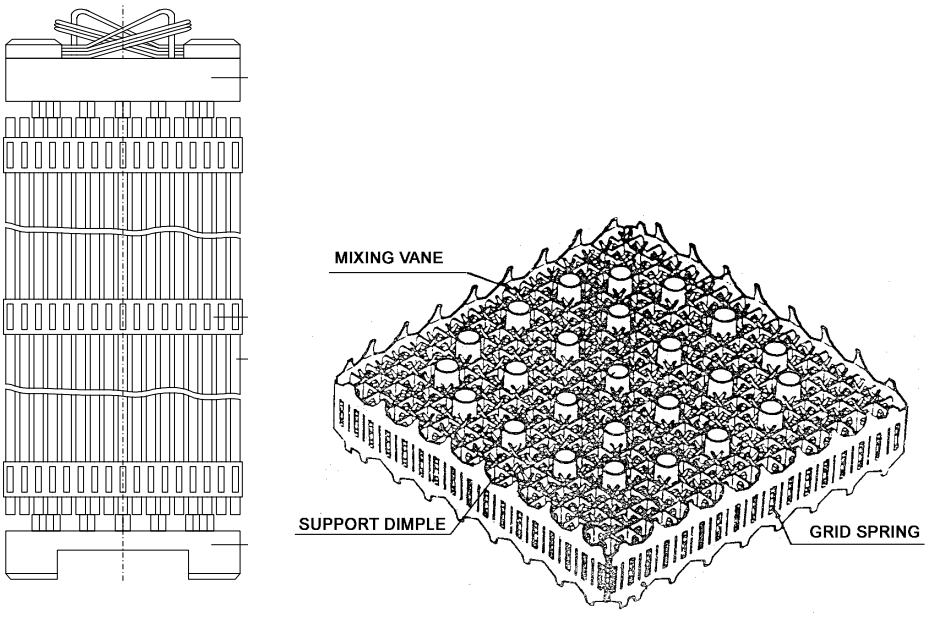

Fig. 1 Illustration of a PWR fuel bundle and grid spacer with the mixing vane

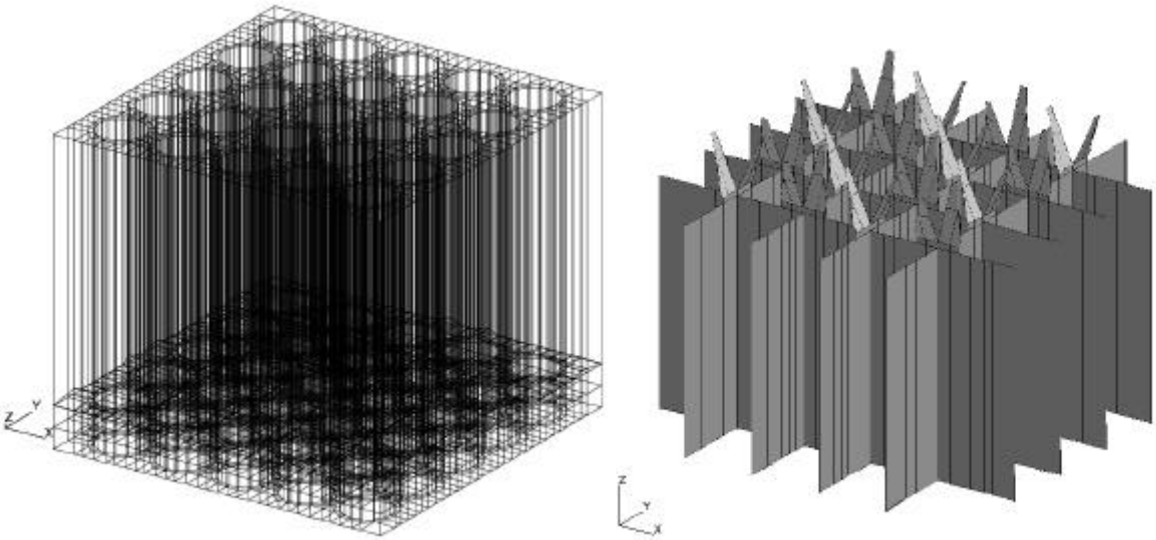

Fig. 2 CFD models of a 5x5 rod array and the split-vane grid

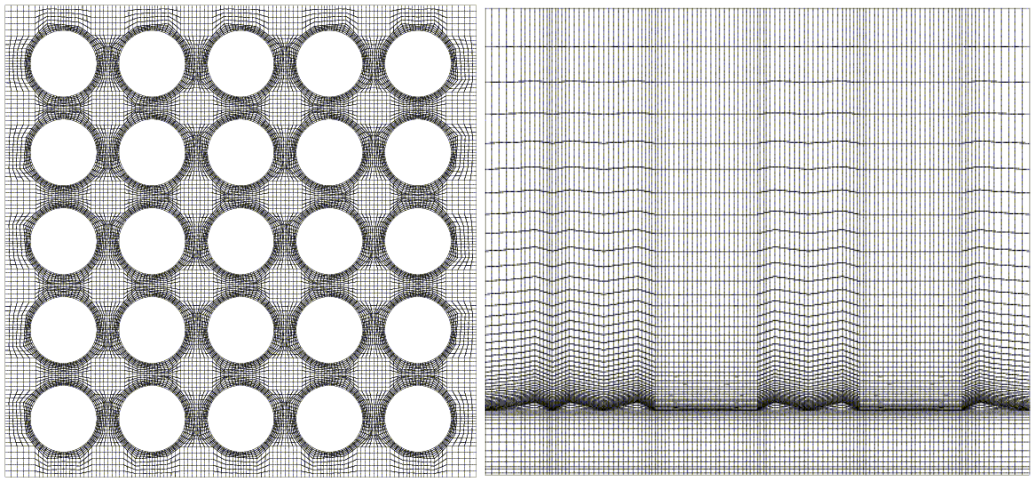

Fig. 3 Cross-sectional (left) and axial (right) meshes for the 5x5 rod array model

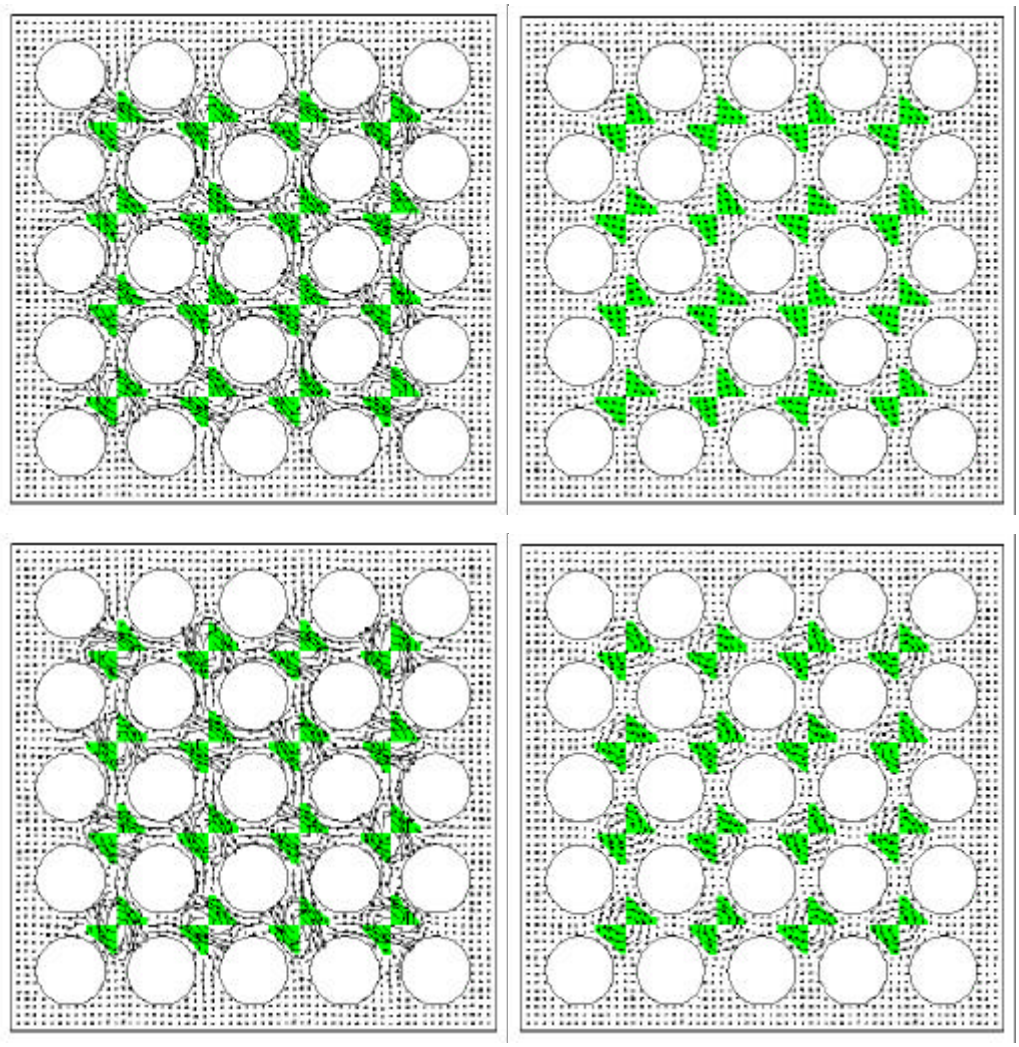

Fig. 4 Velocity vectors 25 mm (left) and 191 mm (right) downstream of the spacer using: (top) standard $k-e$ model and (bottom) DSM

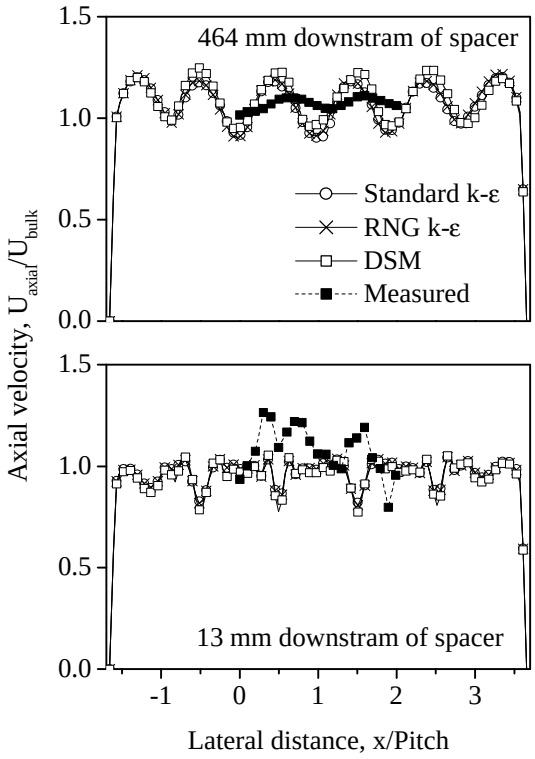

Fig. 5 Comparison of the axial velocity along the centerline of the subchannel (13 mm and 464 mm downstream of the spacer)

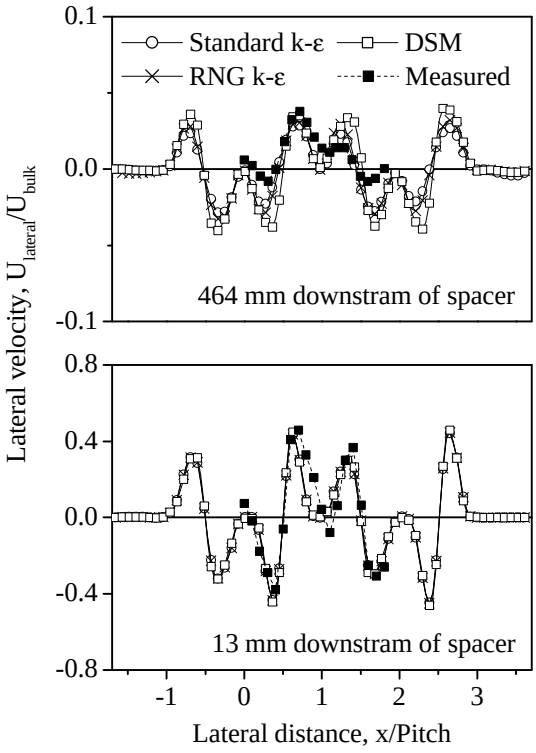

Fig. 6 Comparison of the lateral velocity along the centerline of the subchannel (13 mm and 464 mm downstream of the spacer)

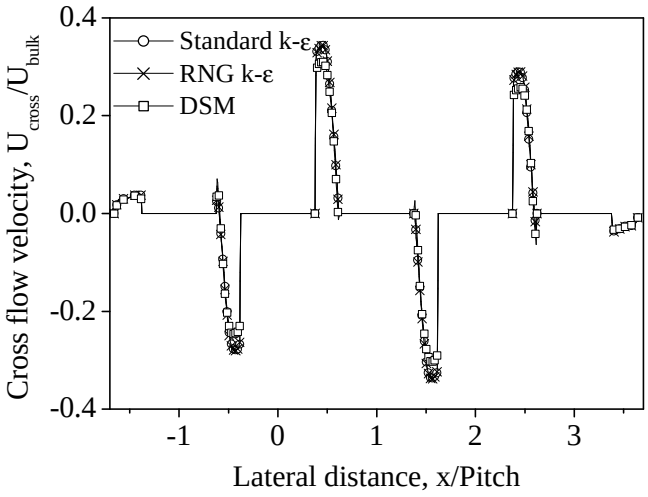

Fig. 7 Comparison of the cross-flow velocity in the gaps (25 mm downstream of the spacer)

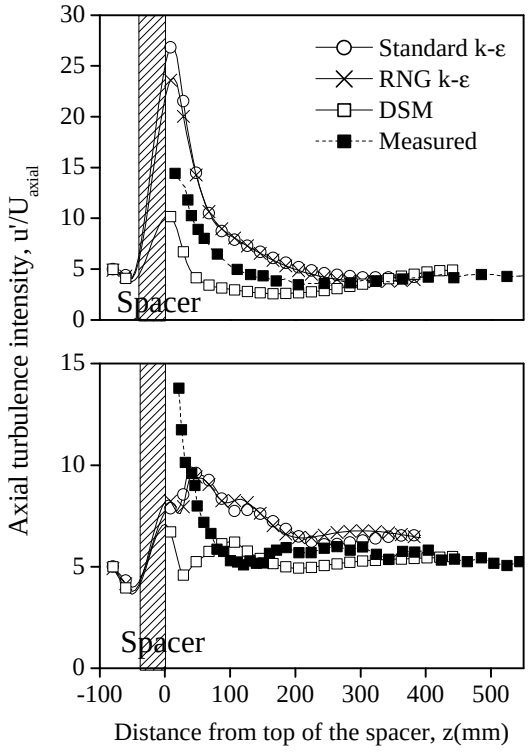

Fig. 8 Axial variations of axial turbulence intensity at the center (top) and the gap (bottom) of the central subchannel